Est. 1984

ORIENTAL JOURNAL OF CHEMISTRY
An International Open Access, Peer Reviewed Research Journal

www.orientjchem.org

ISSN: 0970-020 X
CODEN: OJCHEG
2022, Vol. 38, No.(2):
Pg. 278-285

To Facile the Study of Structural, Morphological Properties of Novel, Synthesised Nano Particles of Indium Doped Ni-Co Ferrite

PATIL JAYSHREE. S, CHANSHETTI UMAKANT. B* and PAWAR CHARUSHILA. B

[1,2]Department of Chemistry, Jawahar College, Andur, Tq. Tuljapur, Osmanabad, Maharashtra, India-413603.
[3]Department of Chemistry, Art's, Commerce and Science College, Ozar (Mig), Tq. Niphad, Nashik, Maharashtra, India-422206.

*Corresponding author E-mail: patiljayshree86@gmail.com

http://dx.doi.org/10.13005/ojc/380207

(Received: January 20, 2022; Accepted: April 18, 2022)

ABSTRACT

Sol-gel technique is used for synthesis of $Ni_{0.5}Co_{0.5}In_xFe_{2-x}O_4$. (x=0.0,0.10,0.075,0.050,0.025) characterized by utilizing. The pre-arranged example sintering temperature is affirmed by TGA. The pre-arranged examples Sintering at 600°C at 4 hours. The Single-phase cubic spinel was affirmed by utilizing the X-beam diffraction (XRD) examination. The underlying boundary like cross lattice constant, porosity, x-beam thickness, hopping length and so on, were estimated by utilizing the XRD information. The lattice constant (a) expanded from 8.347 to 8.378 Å. The x-beam thickness 5.385 to 5.518 g/cm^3 expanded. The floor morphology affirmed through examining SEM. The cation conveyance proposes that Co^{2+}, Ni^{2+}, In^{3+} show a mobility towards the octahedral-B site, Fe^{3+} debris are arbitrarily circulated at the tetrahedral-A and octahedral-B site. The Fourier transform Infrared Spectra (FTIR) of the Ni-Co ferrite framework have been broke down the ingestion power tops both tetrahedral (υ_1) and octahedral (υ_2) increments with expanding the In^{3+} particles.

Keywords: Ni-Co ferrite, Indium, Sol-gel method, SEM, Cation distribution.

INTRODUCTION

Nanocrystalline spinel ferrites having general compound equation MFe_2O_4 (where, M is divalent particle from the 3d series like Ni, Mn, Zn, Cu, and Co) are extremely fascinating attractive materials[1,2]. Spinel ferrites are widely concentrated because of the wild scope of utilizations like inductors, transformers, high-recurrence gadgets, microwave gadgets, multi-facet chip inductors, information stockpiling, and telecom[3–9]. The spinel ferrite is sorted into three distinct sorts Normal spinel, inverse spinel, and random spinel. The inverse spinel is intriguing because of its magneto crystalline like and high saturation magnetization.[10] Ni-C_O ferrite[11,12]. Cobalt-Nickel ferrite shows the inverse spinel structure in which Fe^{+3} and Co^{2+} particles live at both octahedral and tetrahedral destinations while Ni^{2+} particles live just at the octahedral site[3,13-14]. Cobalt and nickel, the two ferrites, have a place with the classification of

inverse spinel ferrites. Fe^{3+} particles supplanted by In^{3+} particles change the grid boundary changed. Because of the relatively larger ionic span of In^{3+} particles (0.8 Å) concerning 3d progress metal particles, indium particles catch octahedral voids and furthermore make create lattice distortions[15-17] a few analysts have given an account of nonmagnetic In^{3+} particles doped ferrite like Co[18,19], Cu[20,21] Ni[22] Ni-Zn[23] Ni-Co[24] Ni-Cu[10] Ni-Cu-Zn[25]. Chandra *et al.,*[26] Concentrated on the $Ni_{0.5}Co_{0.5}Fe_2O_4$ arranged utilizing two unique techniques and its attractive conduct of nanoparticles. K. M. Srinivasa Murthy *et al.,*[27] concentrated on the Union of Ce^{3+} doped Co-Ni ferrites and study the primary, microstructural, and dielectric properties of auto applications. R M Rosnan *et al.,*[28] were researched the expansion of Mg replacement $Co_{0.5}Ni_{0.5-x}Mg_xFe_2O_4$ nanoparticle its practices change in underlying and attractive properties of ferrites. M. Junaid, *et al.,*[10] considered, Effect of indium replacement $Cu_{0.5}Ni_{0.5}Fe_{2-X}O_4$ and improves the dielectric and attractive properties of ferrite. Samrat Mukherjee *et al.,*[24] considered the In^{3+} particle doping on Ni-Co ferrite. The present work considers, $Ni_{0.5}Co_{0.5}Fe_{2-x}InxO_4$. (x=0.0,0.10,0.075,0.050,0.025) ferrite nanoparticles have been arranged by the sol-gel method. The effect of In^{3+} substitute at the structural and Morphology houses of Nickel-Cobalt ferrite has been examined and pointed out exhaustively.

EXPERIMENTAL

Nanocrystalline powder with a synthetic samples $Ni_{0.5}Co_{0.5}Fe_{2-x}InxO_4$ (x=0.0 to 0.025) ferrites were ready using chemical solution deposition method[24]. The Analytical grade reagent was utilized for the blend, for example, Co, Ni, Fe and In nitrate, along with citrus extract ($C_6H_8O_7.H_2O$). The stoichiometric extent of metal nitrate disintegrated in deionized refined water. The molar proportion of 1:3 keeps up with by the expansion of citrus extract arrangement. The pH scale of the subsequent frame-up was modified up to 7, pH by putting liquid alkali, then, at that position the attenuated frame work was heated on the warm plate constantly ageing at 90^{0}C, at last because of auto flaming, brown-hugged detritus was gotten. Pre-arranged examples were sintered at 600^{0}C for 4 hours. The sintering not really settled from TGA/DTA. The power dispersive research of X-beam (EDAX) become carried out to recognize the normal measure of factor and stoichiometry gift in the piece. The X-beam diffraction (XRD) examples of assessments had been recorded at room temperature by means of using Cu–Kα radiation at the Rikagu Miniflag X-beam diffractometer. X-beam diffraction facts had been recorded within the 2θ scope of 20–70° with an inspecting pace of two°/minute. Infrared spectroscopy (IR) estimation changed into finished inside the scope of 800–200 cm^{-1} on a Perkin Elmer infrared Spectrophotometer. The morphological review became finished by using Filtering SEM and became recorded utilizing EDAX Oxford EDAX JEOL–JSM–5600N.

$$(0.5)\ Ni\ (NO_3)_2.6(H_2O) + (0.5)\ Co\ (NO_3)_2.3(H_2O) + (x)\ In(NO_3)_3.9(H_2O) +$$

$$(2\text{-}x)\ Fe\ (NO_3)_2.9(H_2O) + 3C_6H_8O_7$$

$$\downarrow\ pH \cong 7\ (Add\ aq.\ NH_3)$$

$$(Ni_{0.5}Co_{0.5}In_xFe_{2-X}O_4) + 4N_2\uparrow + 2O_2\uparrow + 18Co_2\uparrow + 24H_2O\uparrow$$

RESULT AND DISCUSSION

TGA/DTA

Figure 1 indicates regular (x=0.05) outline of TGA and DSC estimations of arranged powder. TGA and DTA spectra of arranged powder in the whole temperature range 0–1000°C in presence of air. TGA bend indicate mass loss of arranged example because of crumbling of oxides and nitrates. Weight reduction happened in four progressive stages TGA bend it very well may be seen Fig. 1. The top at 103°C was credited by vanishing of assimilated water and the subsequent pinnacle showed up at 144°C ascribed to citrus extract and inorganic mixtures[20]. The sharp abatement in weight reduction top underneath the 330^{o}C is because of metal hydroxides changed over to metal oxide.[29] The gem immaculateness and the warm soundness at temperature 500 to 550^{o}C. Endothermic top in DTA bend at 450^{o}C might sign the development of solidification at spinel stage[25,30]. The last calcination temperature is chosen as 600°C for 4 h of the ferrite being scrutinized.

X-ray diffraction (XRD)

The XRD specimen of toughened $Ni_{0.5}Co_{0.5}Fe_{2-x}InxO_4$ (x=0.0 ,0.10,0.075,0.050,0.025) are displayed in Fig. 2. XRD pinnacle estimated with Bragg's shows from (440), (511), (422), (400), (311), and (220) planes relate to the classic construction.

The acquired x-beam design was filed of all the $Ni_{0.5}Co_{0.5}Fe_{2-x}InxO_4$ tests which are affirmed the development of a homogenous single stage with cubic spinel structure. (JCPDS NO. 01-088-0380)[28]. The orchestrated specimen is of FCC construction with space bundle Fd^3m. The cubic stage gives information of bigger ionic radii of In(III) particle (0.80 Å) contrasted with the Fe^{3+} particles (0.645 Å)[31]. The high centralization of indium might twist the gem cross section and creates extra stage on grain limits. This may be because of the supplanting of more modest particles with bigger particles[20]. The cross-section boundary "a" was determined from the accompanying recipe.

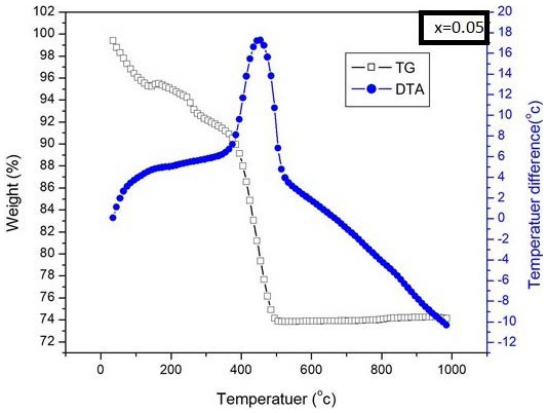

Fig. 1. The expected curve of TGA/DTA of specimen x = 0.05

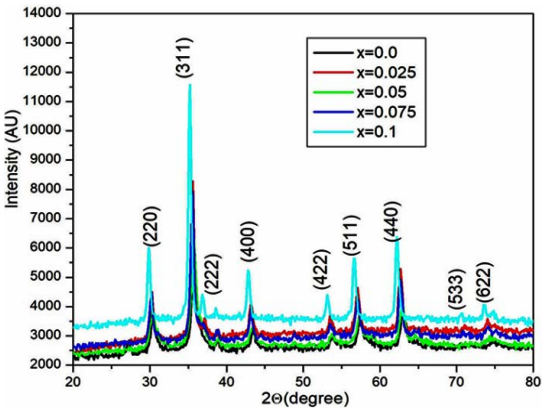

Fig. 2. XRD patterns of $Ni_{0.5}Co_{0.5}Fe_{2-x}InxO_4$. (x=0.0,0.10,0.075,0.050,0.025)

The 'a' was dictated by the connection.[31]

$$a = d\sqrt{(h^2 + k^2 + l^2)} \quad (1)$$

Where, (h, k, l, and a) are Mill operator lists along with d is interplanar separating and steady cross section (a). Estimated upsides of the lattice steady are summarized up. It is observed that the 'a' continuous up rise from 8. 345 Å to 8.378 Å with In^{3+} fixation x. The increments of cross section consistent are arranged in Table 1. The enlargement in cross section consistent are as a result of the variation in ionic radii, the more unpresuming ionic radii of Fe^{3+} (0.645 Å) are supplanted by bigger In^{3+} particle (0.8 Å)[24]. The X-beam thickness (dx) of the specimen was explained by condition.[31]

$$dx = \frac{8M}{Na^3} \quad (2)$$

Where, M, N, a^{3-} are sub-atomic weight of the relating rearrangement, Avogadro's number, volume of unit cell respectively. Upsides of 'dx' bring out in Table 1. It is observed that x-beam densities uprise from 5.292 to 5.791 gcm^{-3} with In^{3+} fixation x, this might be on the base that In^{3+} has more noteworthy nuclear mass m (114 amu) supplant maximal unpresuming Fe^{3+} (55.84amu), and its blowoff enlargements in nuclear load with In^{3+} constituents.[24]

The particle size 't-XRD' of the specimen was estimated utilizing significant pinnacle (311) by Scherrer equation.[31]

$$t_{xrd} = \frac{0.9\lambda}{B\cos\theta} \quad (3)$$

Where, θ, B, λ are Bragg point, full width at half greatest, frequency of radiation respectively. Increment of crystal size are arranged in Table 1. increment of crystal size of the specimen refusd with enlarging the In^{3+} particle content , breadth of nanocrystals was decreased for higher In^{3+} particle rate in Ni-Co nano ferrites. Because of the enormous sweep of In^{3+} (0.8 Å) particles concerning change metal particles, indium particles catch the octahedral voids and furthermore forestalled precious stone development during arrangement.[32] The weight broadness enlarged from 3.023-3.291 (x=0.0-0.1) along expansion in In^{3+} replacement. The potential justification for expanding densities is the presentation of In^{3+}. The P% of the novel ferrite detect by using the equation.[31]

$$P = \left(\frac{d_X - d_B}{d_X}\right) \times 100 \quad (4)$$

Where, dx is X-ray density and dB is bulk density. Percentage porosity (P%) decreased 43.863-40.362%, a boom in In^{3+} content material.

The values of the percentage porosity.

The hopping distance at A and B-sites ((L_A) and (L_B)) were calculated by following equation.

$$L_A = a\sqrt{\frac{3}{4}} \quad (5)$$

$$L_B = a\sqrt{\frac{2}{4}} \quad (6)$$

Hopping lengths (L_A, L_B) the gap between the ions inside the tetrahedral (A) site and octahedral [B] site can be calculated using the relation mentioned someplace else[22]. The values of expected length are given in Table 1. This shows that the expecting period improved with growing In^{3+} ion awareness. The allied parameters along with tetrahedral and octahedral bond length (d_{Ax} and d_{Bx}), tetrahedral aspect, shared and unshared octahedral edge (d_{AXE}, d_{BXE} and d_{BXEU}) were calculated using experiment value 'a', 'u' (zero.375 Å) of lattice constant and oxygen positional parameter respectively by substituting in following equation.

$$d_{Ax}=(u-1/4)a\sqrt{3} \quad (7)$$

$$d_{Bx}=[3u^2-(11/4)\,u+43/64)]^{1/2}.\,a \quad (8)$$

$$d_{AxE}=(2u-1/2)\,a\sqrt{2} \quad (9)$$

$$d_{BxE}=(1-2u)\,a\sqrt{2} \quad (10)$$

$$d_{BxEu}=[4u^2-3u+(11/16)]^{1/2}.a \quad (11)$$

Table 1: Lattice s constant ('a'), X-ray density(dx), Bulk density(dB), Percentage porosity(P), Particle size (DXRD), Hopping lengths(LA and LB) in $Ni_{0.5}Co_{0.5}Fe_{2-x}InxO_4$ Composition

Compound.x	a(obs.) (Å)	Dx(Å)	dB (g/cm^3)	P(%)	DXRD(nm)	LA (Å)	LB(Å)
0.0	8.347	5.3853	3.0231	43.8636	13.132	3.622	2.957
0.025	8.359	5.4105	3.1126	42.4709	13.481	3.626	2.960
0.05	8.365	5.4244	3.1373	42.1633	12.273	3.635	2.968
0.075	8.369	5.4875	3.1914	41.8422	11.077	3.644	2.975
0.01	8.378	5.5179	3.2907	40.3627	10.383	3.646	2.977

The versions of allied parameters with In^{3+} awareness in Ni-Co ferrite is proven in Table 2. The allied parameters are associated with the radii of In^{3+} and Fe^{3+}. The allied parameters are improved with the composition of In^{3+} in Ni-Co ferrite. This boom in aspect lengths arises because of the dopants in doping Incomes and also because of cation distribution inside prepared compositions.

Table 2: x, d_{AX}, d_{BX}, d_{AXE}, d_{BXE} and d_{BXEU} of $Ni_{0.5}Co_{0.5}Fe_{2-x}InxO_4$. (x =0.000,0.100,0.075,0.050,0.025,) Consider, Composition, Tetrahedral bond, Octahedral bond, tetra area, octahedral facet, unshared octahedral area respectively

Compound.x	d_{AX}Å	d_{BX}Å	d_{AXE}Å	d_{BXE}Å	d_{BXEu}Å
0.0	1.8940	2.0379	3.0928	2.8095	2.9528
0.025	1.8967	2.0408	3.0972	2.8135	2.9571
0.05	1.8981	2.0423	3.0994	2.8155	2.9592
0.075	1.8990	2.0433	3.1009	2.8169	2.9606
0.1	1.9010	2.0455	3.1042	2.8199	2.9638

Cation distribution

Cation distributions were decided by studying the X-ray diffraction styles' intensity. The determined intensity ratio changed into compared to the calculated depth ratio on this way. Method of Bertaut[23]. Table 3 suggests the cation distribution of the 600°C samples. The findings display that Ni^{2+}, Co^{2+}, and In^{3+} cations opt to occupy the octahedral positions. The tetrahedral positions are occupied via Fe^{3+} ions[A].[24] The ionic radius for both tetrahedral and octahedral is (rA and rB) and coordinated sites obeying best cationic distribution had been computed using the following relationships[22,24]. Both rA and rB are suggested to remain consistent whereas rB increases with a growth.

$$a_{th} = \frac{8}{3}\sqrt{3}\left[(r_A + R_0) + \sqrt{3}(r_B + R_0)\right] \quad (12)$$

Where, RO denotes the radius of oxygen (RO=1.32), rB and rA denote the radii of the octahedral [B] and tetrahedral (A) sites, respectively. Table 3 summarizes the values of 'a^{th},' and it is able to be proven that the theoretical lattice regular will increase as the quantity of In^{3+} substitution increases[24]. This follows the equal pattern as the experimentally measured lattice parameter (a). The perfect lattice steady (a^{th}) values had been barely higher than the experimental (a) values, which may

be attributed to the atomic image's center premise that atoms are difficult spheres dependent in a positive sample[33]. Using the radius of the oxygen ion RO=1.32 V, the oxygen positional parameter 'u' was calculated[31].

$$u = \left[(r_A + R_0) \frac{1}{\sqrt{3}a} + \frac{1}{4} \right] \quad (13)$$

Table 3 indicates the values of positional oxygen parameters, and this discovered when Ni-CO ferrite is substituted with In^{3+}, the value of 'u' drops. The metallic ions in spinel oxide are lesser than the O_2^- ions. This result shows that the created spinel lattice differed from the genuine spinel lattice by a small amount.[24]

Table .3: x, (ν_1 and ν_2), (rA and rB), (a^{th}), (u) consider as composition, Band role, Cation distribution, Theoretical lattice steady, Oxygen parameter respectively, of $Cu_{0.5}Zn_{0.5}Fe_{2-x}InxO_4$.(x=0.000,0.100,0.075,0.050,0.025)

Compound.x	Cation Distribution		Band Position		Mean ionic radii		a_{th}(Å)	u(Å)
	(A) Site	[B] site	ν_1 cm^{-1}	ν_2 cm^{-1}	rA(Å)	rB (Å)		
0.0	$(Fe^{3+}1)$	$[Ni^{2+}_{0.5}Co^{2+}_{0.5}Fe^{3+}_1]$	576.4	354.19	0.670	0.693	8.430	0.3863
0.025	$(Fe^{3+}1)$	$[Ni^{2+}_{0.5}Co^{2+}_{0.5}Fe^{3+}_{0.975}In^{3+}_{0.025}]$	580.36	358.6	0.670	0.694	8.435	0.3862
0.050	$(Fe^{3+}1)$	$[[Ni^{2+}_{0.5}Co^{2+}_{0.5}Fe^{3+}_{0.950}In^{3+}_{0.05}]$	585.64	369.2	0.670	0.696	8.439	0.3861
0.075	$(Fe^{3+}1)$	$[[Ni^{2+}_{0.5}Co^{2+}_{0.5}Fe^{3+}_{0.925}In^{3+}_{0.075}]$	589.6	395.51	0.670	0.697	8.443	0.3861
0.1	$(Fe^{3+}1)$	$[Ni^{2+}_{0.5}Co^{2+}_{0.5}Fe^{3+}_{0.900}In^{3+}_{0.1}]$	583.21	398.64	0.670	0.699	8.448	0.3860

Fourier Transform Infrared Spectroscopy (FT-IR)

FT-IR conveyance spectra of as-gotten ferrite nanoparticles predicted as recurrence scope of 200-800 cm^{-1} are displayed in Fig. 3. The FT-IR spectra additionally provide facts approximately the scenario of cations inside the gem[34]. FT-IR spectra display two full-size agencies at 576-583.21 and 354.19-398. 64 cm^{-1} that are the trademark band of spinel ferrite. The band 576-583.21 (ν_1) cm^{-1} is identified with the extending vibration of the tetrahedral steel-oxygen bond and 354.19-398.64 cm^{-1} (ν_2) is relating to the octahedral metal-oxygen bond[24,28,34]. It has to be noticed that the pressure of the retention top increments whilst the In^{3+} particles relocated the spinel structure. The outcome may be clarified via the way that the In^{3+} particles may supplant a portion of the Fe^{3+} debris in tetrahedral locations and octahedral locales reinforcing the Fe-O extending vibration.[20,25,28]

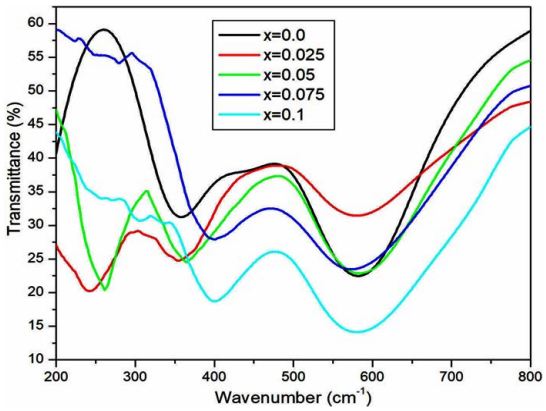

Fig. 3. IR spectrum of $Ni_{0.5}Co_{0.5}Fe_{2-x}InxO_4$. (x=0.0,0.10,0.075,0.050,0.025)

Scanning Electron Microscopy, Energy Dispersive X-ray

The morphological investigation of the pre-arranged examples was dictated by utilizing the Checking electron microscopy (SEM) strategy. The run of the mill SEM pictures is displayed in fig. from Fig. 4. The SEM pictures display that the grains have homogenous dispersion and grains are agglomerated. The agglomerate of ferrite powder framed as a result of the warmness effect; this shows the already arranged specimens are the profoundly responsive and uniform dissemination of grains affirming the translucent design of In^{3+} doped Ni-Co ferrite.[24] The pre-arranged samples' agglomeration is additionally because of the attractive communication between the particles[20,24-25].

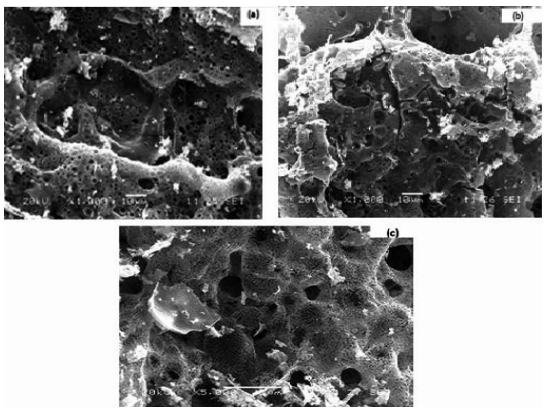

Fig. 4. Typical SEM x=0.0,0.05,0.1 for a, b, c respectively of $Ni_{0.5}Co_{0.5}Fe_{2-x}InxO_4$

The basic organization and their extent were induced by energy dispersive investigation for

In-substituted Ni-Co ferrite tests. EDAX spectra of run of the mill tests of the In-subbed Ni-Co ferrite is displayed in Fig. 5. The presence of pinnacles of the component Co^{2+}, Ni^{2+}, In^{3+}, Fe^{3+}, O_2^- and In^{3+} in EDAX spectra are the affirmation of the development of In-subbed Ni-Co ferrite. The EDAX data obtained from the focal point of In^{3+} subbed ferrite particle of Ni-Co particles showed the existence of a huge grouping of Ni into the power range of 0.8keV, 7.6keV, and 8.2keV, Co in between,0.4keV, 7.2keV, and 7.6keV and Indium was seen somewhere in the range of 2.8keV,3.2keV, and 4.2keV, while Iron was found in between the power range of 0.7 to 6.8 keV.

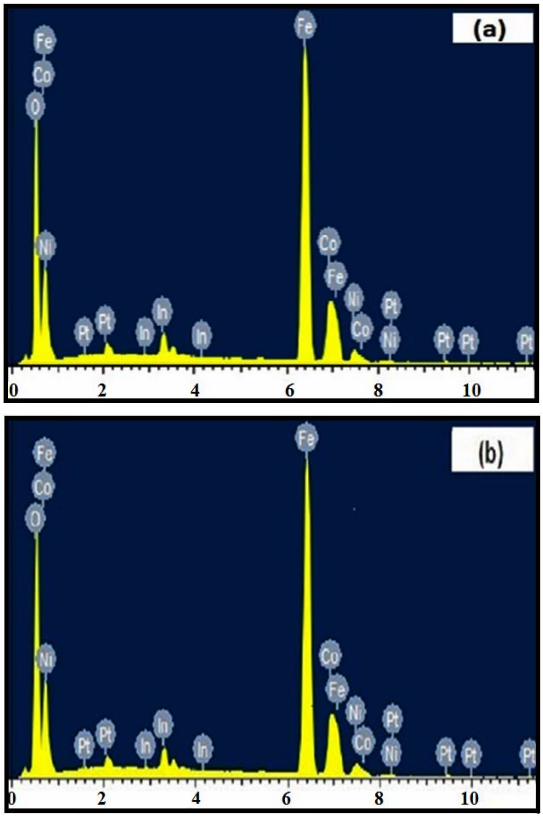

Fig. 5. EDS pattern is x=0.025, x=0.075 for a,b respectively, of $Ni_{0.5}Co_{0.5}Fe_{2-x}InxO_4$ nanoparticles

CONCLUSION

$Ni_{0.5}Co_{0.5}Fe_{2-x}InxO_4$. nanocrystalline ferrite Arranged by Sol-gel strategy. The XRD designs uncovered the development of a cubic spinel structure. TGA examination used to the toughening temperature for arranged powder was assessed. One exothermic pinnacle was seen from DSC investigation. X-beam diffraction examples of the relative multitude of tests had a solitary stage spinel structure. The grid Steady and x-beam thickness builds the normal glasslike size diminished determined from XRD information. The bigger size In^{3+} particles forestall the gem development because of a diminishing in crystallite size with expanding In^{3+} content. The cation dissemination of the In^{3+} particles was entered to octahedral sites[B] and with an increment of Indium rate in Ni-Co nano ferrites. IR spectra affirmed the arrangement of Spinel structure and gave data about the dispersion of particles between the two locales, tetrahedral (A-site) at 576-583.21 cm^{-1} and octahedral (B-site) at 354.19-398. 64 cm^{-1}.The Morphology of the pre-arranged examples was examined by SEM. The normal not set in stone from SEM pictures shows nanometer measurement.

ACKNOWLEDGEMENT

All the authors are gratitude towards to the department of chemistry, Dr Babasaheb Ambedkar Marathwada university also thankful to all the faculty member of ACS College Ojhar Mig.

Conflicts of interest

Present study does not have any conflicts of interest.

REFERENCES

1. Goldman, A.; Modern Ferrite Technology, Marcel Dekker, Inc. New York., **1993**.
2. Gyergyek, S.; Makovec, D.; Kodre, A.; Arčon, I.; Jagodic, M.; Drofenik, M.; Influence of synthesis method on structural and magnetic properties of cobalt ferrite nanoparticles. *Journal of Nanoparticle Research*., **2010,** *12* (4), 1263-73.
3. Smit, J.; Wijin, H.P.J,; Ferrites Philips Technical Library. Eindhoven., **1959**.
4. Atif, M.; Nadeem, M.; Grössinger R, Turtelli RS. Studies on the magnetic, magneto strictive and electrical properties of sol-gel synthesized Zn doped nickel ferrite. *Journal of Alloys and Compounds*., **2011**, *509*(18), 5720-4.

5. Gyergyek, S.; Makovec, D.; Kodre, A.; Arčon, I.; Jagodič, M.; Drofenik, M.; Influence of synthesis method on structural and magnetic properties of cobalt ferrite nanoparticles. *Journal of Nanoparticle Research*., **2010,** *12* (4), 1263-73.
6. Jie, S.; Lixi, W.; Naicen, X.; Zhang, Q.; Microwave electromagnetic and absorbing properties of Dy^{3+} doped Mn-Zn ferrites. *Journal of Rare Earths*., **2010**, *28*(3), 451-5.
7. Peng, J.; Hojamberdiev, M.; Xu, Y.; Cao, B.; Wang, J.; Wu, H.; Hydrothermal synthesis and magnetic properties of gadolinium-doped $CoFe_2O_4$ nanoparticles. *Journal of Magnetism and Magnetic Materials*., **2011**, *323*(1), 133-7.
8. Niu, Z.P.; Wang, Y.; Li, F.S.; Magnetic properties of nanocrystalline Co–Ni ferrite. *Journal of materials science*., **2006**, *41*(17), 5726-30.
9. Almessiere, M.A.; Ünal, B.; Slimani, Y.; Korkmaz, A.D.; Baykal, A.; Ercan, I.; Electrical properties of La^{3+} and Y^{3+} ions substituted $Ni_{0.3}Cu_{0.3}Zn_{0.4}Fe_2O_4$ nanospinel ferrites. *Results in Physics*., **2019**, *15*, 102755.
10. Junaid, M.; Khan, M.A.; Akhtar, M.N.; Hussain, A.; Warsi, M.F.; Impact of indium substitution on dielectric and magnetic properties of $Cu_{0.5}Ni_{0.5}Fe_{2-x}O_4$ ferrite materials. *Ceramics International.,* **2019**, *45*(10), 13431-37.
11. Ghosh, M.P.; Kumar, P.; Kar, M.; Mukherjee, S.; Impact of In^{3+} ion substitution on microstructural, magnetic and dielectric responses of nickel–cobalt spinel ferrite nanocrystals. *Journal of Materials Science: Materials in Electronics*., **2020**, *31*(20), 17762-72.
12. Lassoued, A.; Li, J.F.; Magnetic and photocatalytic properties of Ni–Co ferrites. *Solid State Sciences*., **2020**, *104*, 106199.
13. Mohan, R.; Ghosh, M.P.; Mukherjee, S.; Size dependent exchange bias in single-phase $Zn_{0.3}Ni_{0.7}Fe_2O_4$ ferrite nanoparticles. *Journal of Magnetism and Magnetic Materials*., **2018**; *458*, 193-9.
14. Zhao, L.; Yang, H.; Yu, L.; Cui, Y.; Zhao, X.; Feng, S.; Magnetic properties of Re-substituted Ni–Mn ferrite nano crystallites. *Journal of materials science*., **2007**, *42*(2), 686-91.
15. Shirsath, S.E.; Toksha, B.G.; Jadhav, K.M.; Structural and magnetic properties of In^{3+} substituted $NiFe_2O_4$. *Materials Chemistry and Physics*., **2009**, *117*(1), 163-8.
16. Coey, J.M.; Magnetism and magnetic materials. Cambridge university press., **2010**.
17. Aggarwal, A.; Thakur, G.S.; Techniques of performance appraisal-a review. *International Journal of Engineering and Advanced Technology (IJEAT).,* **2013**, *2*(3), 617-21.
18. Nongjai, R.; Khan, S.; Asokan, K.; Ahmed, H.; Khan, I.; Magnetic and electrical properties of In doped cobalt ferrite nanoparticles. *Journal of Applied Physics*., **2012**, *112*(8), 084321.
19. Gerardin, R.; Alebouyeh , A.; Brice, JF.; Evrard, O.; Sanchez, J.P.; Distribution cation que dans les ferrites d'indium de type spinelle InMFeO4 (M=Ni, Mn, Co, Mg). *Journal of Solid-State Chemistry*., **1988**, *76*(2), 398-406.
20. Junaid, M.; Khan, M.A.; Abubshait, S.A.; Akhtar, M.N.; Kattan, N.A.; Laref, A.; Javed, H.M.; Structural, spectral, dielectric and magnetic properties of indium substituted copper spinel ferrites synthesized via sol gel technique. *Ceramics International*., **2020**, *46* (17), 27410-8.
21. Manikandan, V.; Singh, M.; Yadav, B.C.; Vigneselvan, S.; Room-temperature gas sensing properties of nanocrystalline-structured indium-substituted copper ferrite thin film. *Journal of Electronic Materials*., **2018**, *47*(11), 6366-72.
22. Thakur, S.; Katyal, S.C.; Gupta, A.; Reddy, V.R.; Singh, M.; Room temperature ferromagnetic ordering in indium substituted nano-nickel-zinc ferrite. *Journal of Applied Physics*., **2009**, *105*(7), 07A521.
23. Zhu, J.F.; Chen, M.N.; Ke, S.D.; Feng, S.J.; Magnetic properties of indium doped $Ni_{0.4}Zn_{0.6}InxFe_{2-x}O_4$. *Materials Research Express*., **2019**, *6*(11), 116127.
24. Ghosh, M.P.; Kumar, P.; Kar, M.; Mukherjee, S.; Impact of In^{3+} ion substitution on microstructural, magnetic and dielectric responses of nickel–cobalt spinel ferrite nanocrystals. *Journal of Materials Science: Materials in Electronics*., **2020,** *31*(20), 17762-72.
25. Hashim, M.; Shirsath, S.E.; Kumar, S.; Kumar, R.; Roy, A.S.; Shah, J.; Kotnala, R.K.; Preparation and characterization chemistry of nano-crystalline Ni–Cu–Zn ferrite. *Journal of alloys and compounds*., **2013**, *549*, 348-57.
26. Choudhary, B.L.; Kumar, U.; Kumar, S.; Chander, S.; Kumar, S.; Dalela, S.; Dolia, S.N.; Alvi, P.A.; Irreversible magnetic behaviour with temperature variation of $Ni_{0.5}Co_{0.5}Fe_2O_4$ nanoparticles. *Journal of Magnetism and Magnetic Materials*., **2020**, *507*, 166861.

27. Srinivasa, Murthy, K.M.; Angadi, V.J.; Kumar, P.M.; Nagaraj, B.S.; Deepthi, P.R.; Pasha, UM.; Rudra, swamy, B.; Synthesis and study of structural, microstructural and dielectric properties of Ce^{3+} doped Co-Ni ferrites for automotive applications. *In AIP Conference Proceedings AIP Publishing LLC.*, **2018**, *1953* (1), 030277.
28. Rosnan, R.M.; Othaman, Z.; Hussin, R.; Ati, A.A.; Samavati, A.; Dabagh, S.; Zare, S.; Effects of Mg substitution on the structural and magnetic properties of $Co_{0.5}Ni_{0.5-x}Mg_x Fe_2O_4$ nanoparticle ferrites. *Chinese Physics B.*, **2016**, *25*(4), 047501.
29. Garcia-Cerda, L.A.; Rodrıguez-Fernández, O.S.; Reséndiz-Hernández, P.J.; Study of Sr-Fe synthesized by the sol–gel method. *Journal of alloys and compounds.*, **2004**, *369*(12), 182-4.
30. De, Vidales, J. M.; López-Delgado, A.; Vila, E.; Lopez, F.A.; The effect of the starting solution on the physico-chemical properties of zinc ferrite synthesized at low temperature. *Journal of Alloys and Compounds.*, **1999**, *287* (1), 276-83.
31. Cullity, B.D.; Elements of X-ray Diffraction. Addison-Wesley Publishing., **1956**.
32. Shannon, R.D.; Revised effective ionic radii and systematic studies of interatomic distances in halides and chalcogenides. Acta crystallo graphical section A: crystal physics, diffraction, theoretical and general crystallography., **1976**, *32*(5), 751-67.
33. Lakhani, V.K.; Pathak, T.K.; Vasoya, N.H.; Modi, K.B.; Structural parameters and X-ray Debye temperature determination study on copper-ferrite-aluminates. *Solid State Sciences.*, **2011**, *13*(3), 539-47.
34. Waldron RD; Infrared spectra of ferrites. *Physical review.*, **1955,** 15;*99*(6), 1727.